Supporting Information

Three-in-one cathode host based on superlattice Nb_3O_8/graphene heterostructures for high-performance Li–S batteries

*Chenhui Wang[a], Nobuyuki Sakai[a], Yasuo Ebina[a], Takayuki Kikuchi[a], Monika R. Snowdon[b], Daiming Tang[a], Renzhi Ma[a], and Takayoshi Sasaki[a]**

[a] *International Center for Materials Nanoarchitectonics (WPI-MANA), National Institute for Materials Science (NIMS), Namiki 1-1, Tsukuba, Ibaraki, 305-0044, Japan.*

[b] *Department of Chemistry, Faculty of Science, Waterloo Institute of Nanotechnology, University of Waterloo, Waterloo, ON, N2L 3G1, Canada.*

** Corresponding author, E-mail: SASAKI.Takayoshi@nims.go.jp*

Experimental Section

Materials: Potassium nitrate (KNO_3, 99.0%, Kanto Chemical), niobium oxide (Nb_2O_5, 99.99%, Rare Metallic), nitric acid (HNO_3, 60%, FUJIFILM Wako Pure Chemical), tetrabutylammonium hydroxide solution (TBAOH, 10 wt%, Wako special grade, FUJIFILM Wako Pure Chemical), poly(diallyldimethylammonium) chloride (PDDA, 20 wt% in water, Aldrich), graphite power (FUJIFILM Wako Pure Chemical), potassium permanganate ($KMnO_4$, FUJIFILM Wako Pure Chemical), sulfuric acid (H_2SO_4, 95.0 wt%, guaranteed reagent, FUJIFILM Wako Pure Chemical), hydrogen peroxide (H_2O_2, 30%, guaranteed reagent, FUJIFILM Wako Pure Chemical), hydrochloric acid (HCl, 35%, Kishida Chemical), hydrazine monohydrate ($N_2H_4{\cdot}H_2O$, 98 wt%, 98%+, Kishida Chemical), sulfur (S, 99.998%, Aldrich), lithium bis(trifluoromethanesulfonyl)imide (LiTFSI, 99.95%, Aldrich), lithium nitrate ($LiNO_3$, SAJ first grade, Sigma-Aldrich), 1,2-dimethoxyethane (DME, 99.5%, Sigma-Aldrich), 1,3-dioxolane (DOL, 99.8%, Sigma-Aldrich), *N*-methyl-2-pyrrolidone (NMP, 99.0%, FUJIFILM Wako Pure Chemical), conductive carbon black (Super P, 99+% Alfa Aesar), polyvinylidene fluoride (PVDF, average Mw ~534000, Aldrich), lithium foil (Li, 99.8%, Alfa Aesar), lithium

sulfide (Li_2S, 99.98%, Aldrich), and tetraglyme (99.9%, Sigma-Aldrich). These materials were used as purchased.

Preparation of the Nb_3O_8 nanosheet suspension and its restacked form: Nb_3O_8 nanosheets were prepared according to previous reports with some modifications.[1] First, KNb_3O_8 was synthesized by a high-temperature solid-state reaction. KNO_3 and Nb_2O_5 were mixed at a molar ratio of 2:3 and intimately ground for 30 min. Then, the mixture was precalcined at 600 °C for 2 h and then 900 °C for 2 h. After cooling, the mixture was ground for another 30 min and calcined at 900 °C for 20 h to produce KNb_3O_8. Obtained KNb_3O_8 (10 g) was immersed in HNO_3 (2 mol L^{-1}, 1 L) and stirred for 3 days; the solution was changed every 24 h by decantation. The resultant HNb_3O_8 (4 g) was dispersed and delaminated in tetrabutylammonium hydroxide (TBAOH) aqueous solution (1 L) with a molar ratio of TBA^+:H^+ = 1:1. After shaking for 10 days at 180 rpm, the sample was centrifuged at 2000 rpm for 10 min to remove the unexfoliated niobate. The resulting sample was centrifuged again at 20000 rpm for 30 min to recover the nanosheets. After washing with deionized water several times until the supernatant became neutral, the nanosheets were dispersed in water to produce a colloidal suspension of Nb_3O_8 nanosheets. The Nb_3O_8 nanosheet suspension was centrifuged at 20000 rpm for 30 min, and the sediment was freeze-dried to obtain restacked Nb_3O_8 nanosheets.

Preparation of the PDDA-modified reduced graphene oxide (*rGO) suspension, original reduced graphene oxide suspension and restacked rGO nanosheets*: Graphite oxide was synthesized by the modified Hummers' method from graphite powder.[2] $KMnO_4$ (3 g) was slowly added into a mixture of graphite powder (1 g) and H_2SO_4 (25 mL) in an ice bath, and the temperature was kept below 4 °C. After stirring for 2 h, the mixture was stirred at 35 °C for another 3 h. Then, H_2O (46 mL) was added dropwise and stirred for 1 h at 100 °C. H_2O (70 mL) and H_2O_2 (10 mL) were added in sequence and stirred for 1 h. The mixture was centrifuged (5000 rpm for 30 min) and washed with HCl (1 mol L^{-1}) three times and then washed with water

until the supernatant became neutral. The obtained graphite oxide was exfoliated and dispersed in water by ultrasonic treatment. The resulting suspension was centrifuged at 5000 rpm for 30 min to remove unexfoliated graphite oxide. The top solution was further centrifuged at 20000 rpm for 30 min, and the recovered sediment was dispersed in H_2O to obtain a suspension of graphene oxide (GO). The GO suspension (0.2 g L^{-1}, 1 L) was mixed with a PDDA solution (20 wt%, 7.5 mL) and hydrazine monohydrate (98 wt%, 15 μL) and kept at 90 °C for 3 h.[3] The sample underwent repeated centrifugation (20000 rpm for 30 min) and washing with water until the supernatant was neutral. Then, a suspension of PDDA-modified reduced graphene oxide (rGO) was obtained by dispersing the sediment in H_2O. A suspension of pristine rGO without PDDA modification was prepared by the same method without the addition of PDDA. The suspension was used to prepare a randomly restacked material of Nb_3O_8 nanosheets and rGO. The suspension of PDDA-modified rGO was centrifuged at 20000 rpm for 30 min, and the sediment was freeze-dried to produce restacked rGO nanosheets.

Calculation of the mass ratio of rGO to the Nb_3O_8 nanosheet for superlattice assembly: The mass ratio of rGO to the Nb_3O_8 nanosheet was calculated on the basis of the hypothetical area-matching model to maximize the interfacial area of the two types of nanosheets.[4] The in-plane structures of graphene and Nb_3O_8 nanosheets are the hexagonal unit cell of a (0.25 nm) and the rectangular unit cell of a (0.89 nm) × c (0.38 nm),[5] respectively. Thus, the 2D weight densities of the graphene nanosheet ($W_{graphene}$) and Nb_3O_8 nanosheet (W_{Nb3O8}) are $2M$ (C)/(a × a × sin120°N_A) and $2M$ (Nb_3O_8)/(a × c × N_A), respectively, wherein N_A is Avogadro's number and M (C) and M (Nb_3O_8) are the molecular weights of carbon and Nb_3O_8, respectively. The mass ratio of rGO to Nb_3O_8 is estimated as $W_{graphene}$ / W_{Nb3O8}= 0.185 based on an area balance of 1:1.

Fabrication of superlattice Nb_3O_8/rGO (S-Nb_3O_8/rGO) and randomly restacked Nb_3O_8/rGO (R-Nb_3O_8/rGO): A Nb_3O_8/rGO (S-Nb_3O_8/rGO) superlattice composite was prepared by the self-assembly flocculation method with the suspensions of positively charged PDDA-modified

rGO and negatively charged Nb_3O_8 nanosheets.[6] The same volume of the suspensions of PDDA-modified rGO (0.1 g L^{-1}, pH=9) and Nb_3O_8 nanosheet (0.54 g L^{-1}, pH=9) was added dropwise to water (pH=9) at the same speed under stirring. The Nb_3O_8/rGO superlattice composite (S-Nb_3O_8/rGO) was obtained by centrifuging at 5000 rpm for 10 min, washing with deionized water three times, and freeze-drying. The same volume of the suspensions of Nb_3O_8 nanosheets (0.54 g L^{-1}) and original rGO (0.1 g L^{-1}) was directly poured into a PDDA solution (10 g L^{-1}). The resulting solution was centrifuged at 5000 rpm for 30 min, and the sediment was freeze-dried to obtain a randomly restacked Nb_3O_8/rGO sample (R-Nb_3O_8/rGO). The restacked Nb_3O_8 nanosheets, restacked rGO nanosheets, and R-Nb_3O_8/rGO were used as control samples.

Materials characterization: X-ray diffraction (XRD) patterns were recorded on a powder diffractometer (Rigaku Rint-2200) at a scan range of 2° - 90° using a Cu Kα radiation source (λ = 1.5405 Å). Thermogravimetric analysis was carried out with Rigaku TG-DTA8122. The morphology of the materials was observed by scanning electron microscopy (SEM, JEOL Ltd. JSM-6700F) equipped with energy-dispersive X-ray spectroscopy (EDS) and transmission electron microscopy (TEM, JEOL Ltd. JEM-3000F). X-ray photoelectron spectroscopy (XPS) was recorded by an XPS spectrometer (ULVAC-PHI. Inc. Quantum-2000). The ultraviolet-visible absorption spectra were collected with an ultraviolet-visible spectrophotometer (UV-Vis, Hitachi U-4100). Raman spectra were obtained by a Raman spectrometer (HORIBA Jobin Yvon, T64000).

Preparation of sulfur cathode materials: Sulfur cathode materials were prepared by the melting-diffusion method. Host materials (rGO, Nb_3O_8, R-Nb_3O_8/rGO, and S-Nb_3O_8/rGO) and sulfur at a mass ratio of 3:7 were ground for 30 min. Then, the mixture was kept at 155 °C for 15 h in an argon atmosphere to obtain sulfur cathode materials. The sulfur cathode materials prepared with host materials of rGO, Nb_3O_8, R-Nb_3O_8/rGO, and S-Nb_3O_8/rGO powder were named S@rGO, S@Nb_3O_8, S@R-Nb_3O_8/rGO, and S@S-Nb_3O_8/rGO, respectively.

Cathode fabrication for lithium sulfur batteries: Sulfur cathode materials (S@rGO, S@Nb_3O_8, S@R-Nb_3O_8/rGO, and S@S-Nb_3O_8/rGO), conductive carbon black (Super P), and binder (polyvinylidene fluoride, PVDF) at a mass ratio of 7:2:1 were mixed and then dispersed in NMP to form a slurry. Then, the slurry was coated on a carbon-coated aluminum foil via a doctor blade. After drying at 60 °C under vacuum for 12 h and being cut into disks, obtained electrodes with a diameter of 14 mm were used to assemble lithium-sulfur batteries. The host electrodes (rGO, Nb_3O_8, R-Nb_3O_8/rGO, and S-Nb_3O_8/rGO) for blank batteries and symmetric batteries were prepared in the same way with host materials instead of sulfur-host materials.

Electrochemical measurement: The electrochemical tests were conducted on an electrochemical workstation (Solartron, 1280B) and carried out with CR2032 coin cells, which were assembled in an argon-filled glove box. The lithium-sulfur batteries were fabricated with cathodes, separator (Celgard 2325), lithium foil anodes, and an electrolyte of 1 mol L^{-1} LiTFSI with 2 wt% $LiNO_3$ in DME/DOL (1:1 in volume). The sulfur loading and electrolyte/sulfur ratio of lithium-sulfur batteries were ~1 mg cm^{-2} and 19 µl/mg. The charge/discharge performance of lithium-sulfur batteries was examined on a charge/discharge system (Hokuto, HJ1001SD8) in the voltage range of 1.7 - 2.8 V. The rate performance of lithium-sulfur batteries was measured based on the capacity of 1675 mAh g^{-1} at 1C.

Study of the kinetics of lithium polysulfide conversion: Li_2S_6 symmetric cells were assembled with the host electrodes acting as both the working and counter electrodes, wherein a Celgard 2325 separator and a 0.2 mol L^{-1} Li_2S_6 + 1 mol L^{-1} LiTFSI + 2 wt% $LiNO_3$ in DOL/DME (1:1 in volume) electrolyte were used. The electrolytes were prepared by adding S and Li_2S at a molar ratio of 5:1, LiTFSI, and $LiNO_3$ into a solution of DME/DOL (1:1 in volume) and stirring for 48 h at 60 °C. Cyclic voltammetry (CV) and electrochemical impedance spectroscopy (EIS) tests of the Li_2S_6 symmetrical cells were conducted on an electrochemical workstation (Solartron, 1280B).

Study of Li_2S Nucleation: Li_2S_8 cells were assembled with a cathode (host electrode), anode (lithium foil), separator (Celgard 2325), electrolyte (catholyte: 0.3 mol L^{-1} Li_2S_8 + 1.0 mol L^{-1} LiTFSI in tetraglyme, anolyte: tetraglyme) to examine the Li_2S nucleation kinetics. The coin cells were first discharged to 2.06 V at 112 μA and then kept at a voltage of 2.05 V by an electrochemical workstation (Solartron, 1280B). The catholyte was prepared by adding S and Li_2S at a molar ratio of 7:1 and LiTFSI into DOL/DME (1:1 in volume) and stirring for 48 h at 60 °C.

Lithium polysulfide adsorption test: A solution of 0.005 mol L^{-1} Li_2S_6 in DOL/DME (1:1 in volume) (4 mL) was mixed with 15 mg of host material (R-Nb_3O_8/rGO or S-Nb_3O_8/rGO) to examine the adsorption capacity.

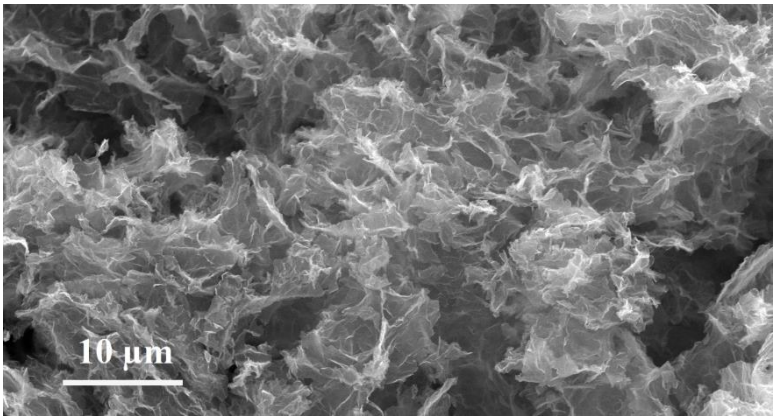

Figure S1. SEM image of S-Nb_3O_8/rGO.

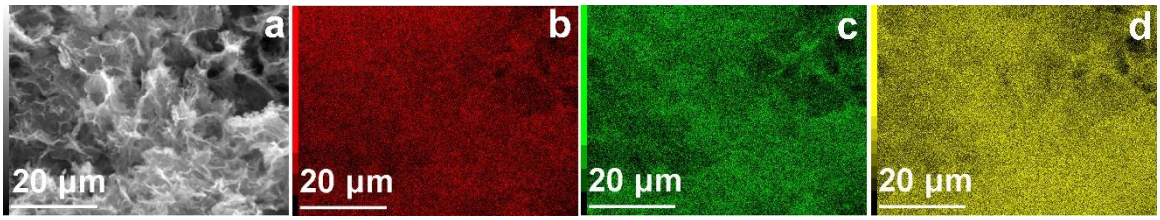

Figure S2. a) SEM image of S-Nb_3O_8/rGO and EDS mapping of b) C, c) O, and d) Nb.

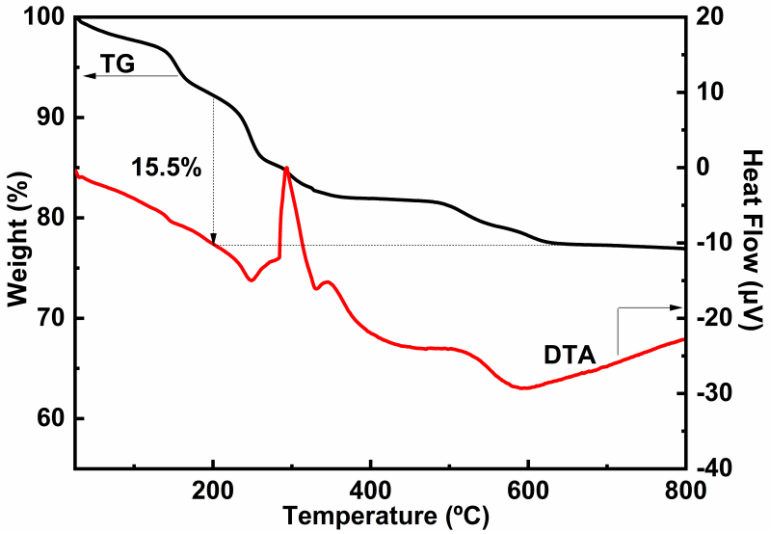

Figure S3. TG and DTA curves of restacked Nb_3O_8 nanosheets in air.

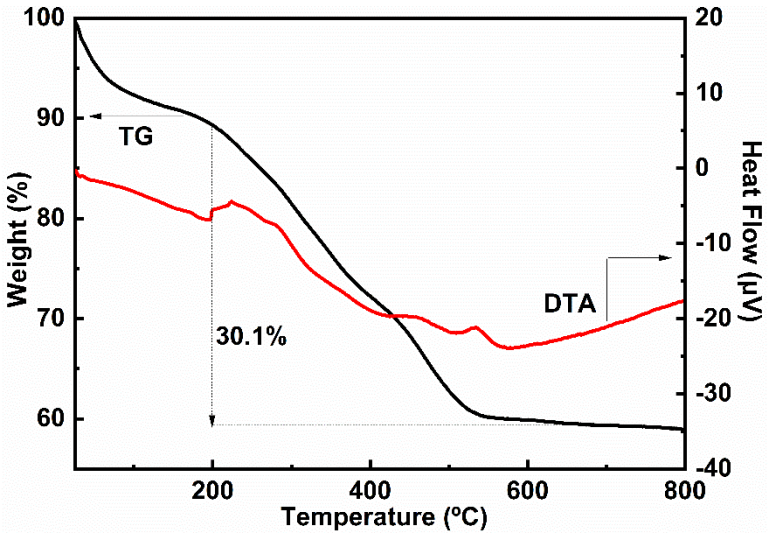

Figure S4. TG and DTA curves of S-Nb_3O_8/rGO.

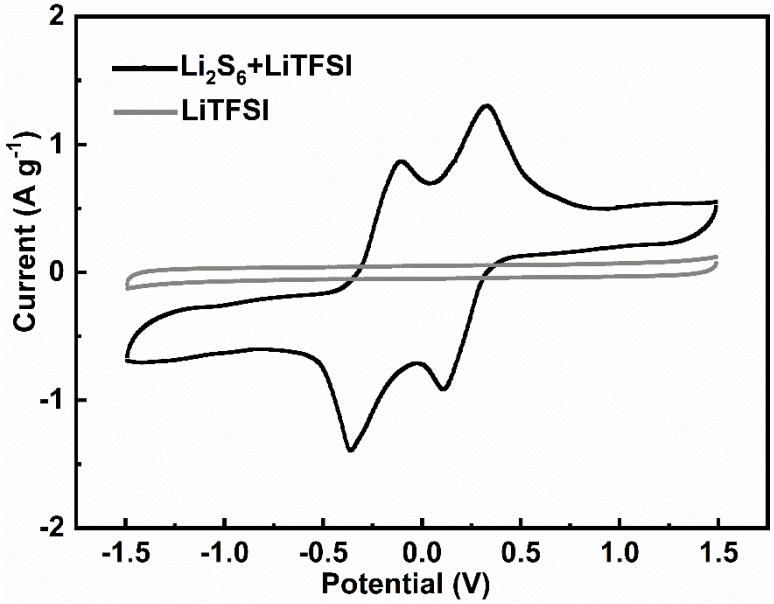

Figure S5. CV curves of the rGO symmetric battery at a scan rate of 1 mV s^{-1} in the presence and absence of Li_2S_6.

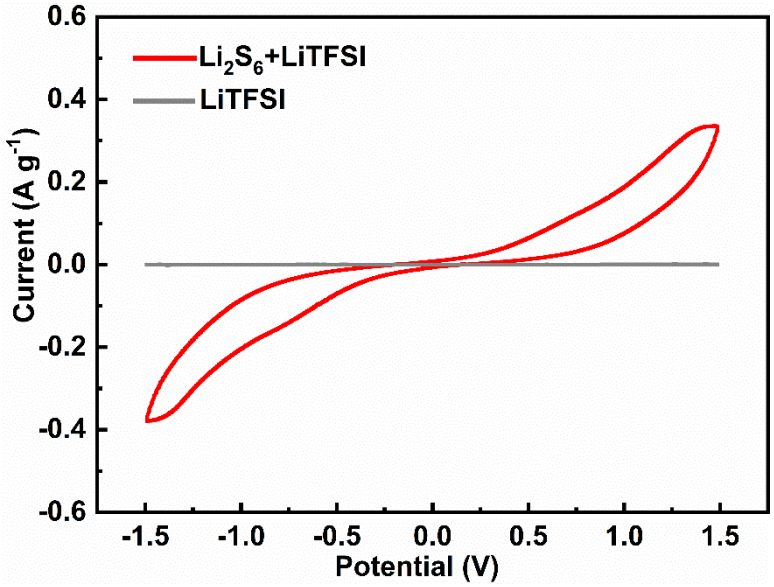

Figure S6. CV curves of the Nb_3O_8 nanosheet symmetric battery at a scan rate of 1 mV s^{-1} in the presence and absence of Li_2S_6.

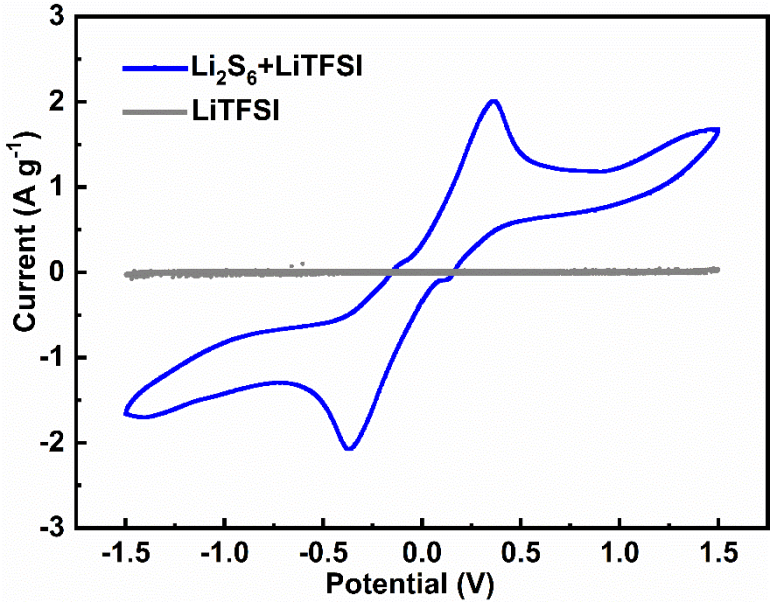

Figure S7. CV curves of the R-Nb_3O_8/rGO symmetric battery at a scan rate of 1 mV s^{-1} in the presence and absence of Li_2S_6.

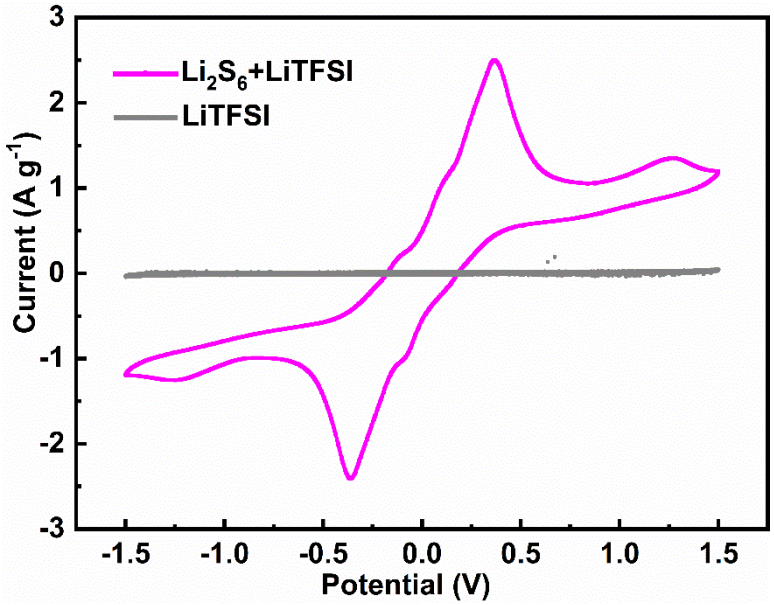

Figure S8. CV curves of the S-Nb_3O_8/rGO symmetric battery at a scan rate of 1 mV s^{-1} in the presence and absence of Li_2S_6.

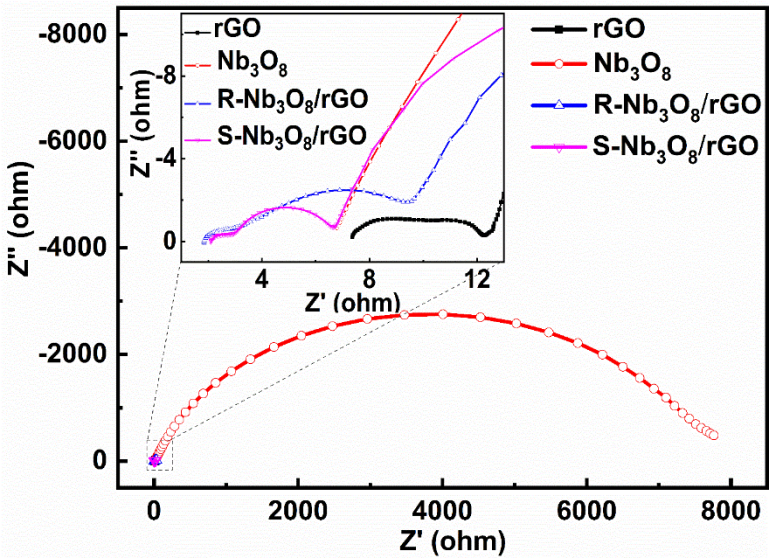

Figure S9. EIS of the rGO, Nb_3O_8 nanosheet, R-Nb_3O_8/rGO and S-Nb_3O_8/rGO Li_2S_6 symmetric batteries.

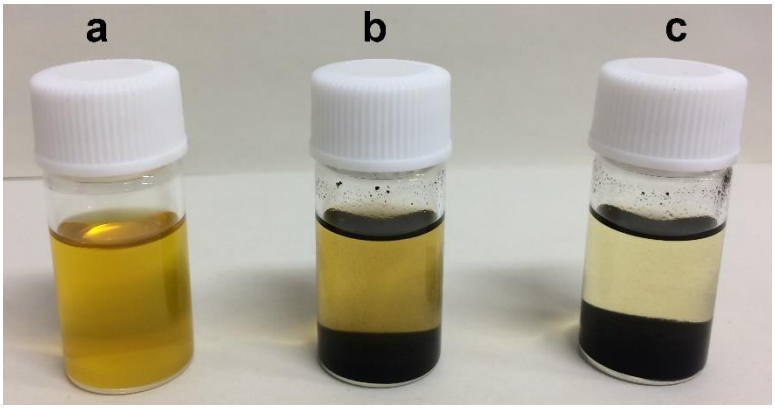

Figure S10. Photograph of a) 0.005 M Li_2S_6 in DOL/DME (V_{DOL}:V_{DME} = 1:1) (4 mL) and then after mixing with b) R-Nb_3O_8/rGO (15 mg) and c) S-Nb_3O_8/rGO (15 mg).

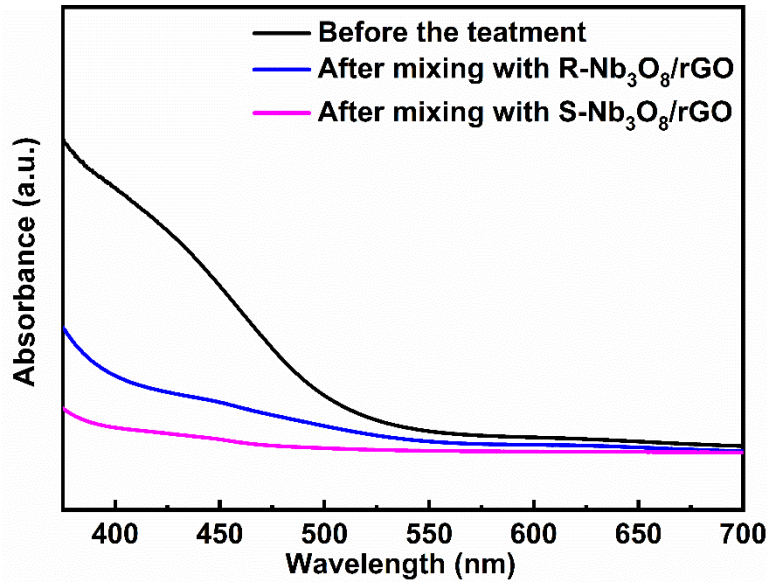

Figure S11. UV-Vis spectra of the Li_2S_6 electrolyte before and after being mixed with R-Nb_3O_8/rGO and S-Nb_3O_8/rGO.

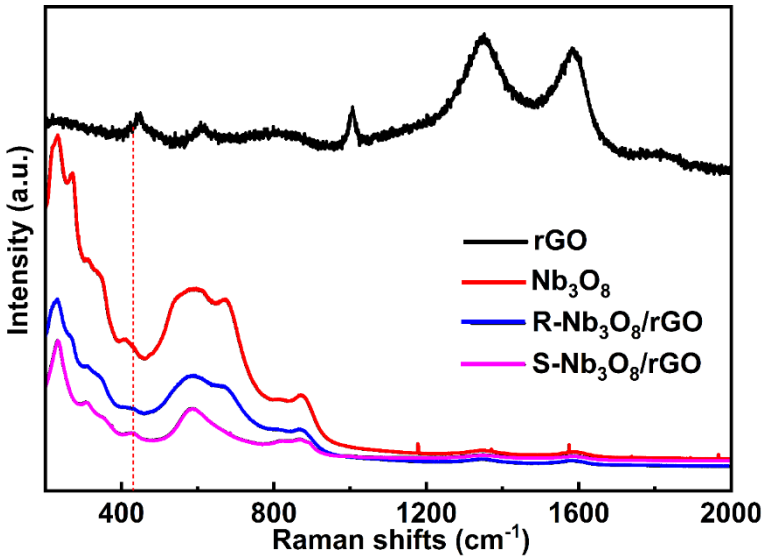

Figure S12. Raman spectra of the rGO, Nb_3O_8 nanosheet, R-Nb_3O_8/rGO and S-Nb_3O_8/rGO electrodes after the potentiostatic process.

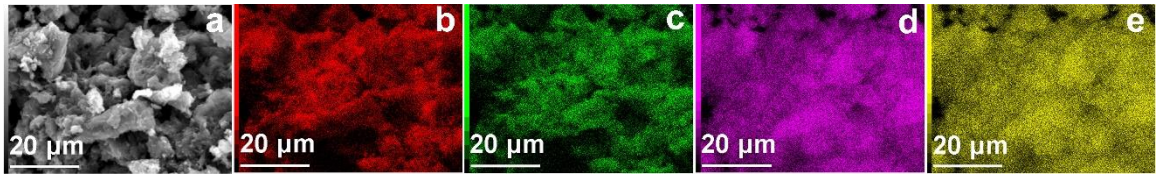

Figure S13. a) SEM image of the S-Nb_3O_8/rGO electrode after the potentiostatic process and EDS mapping of b) C, c) O, d) Nb, and e) S.

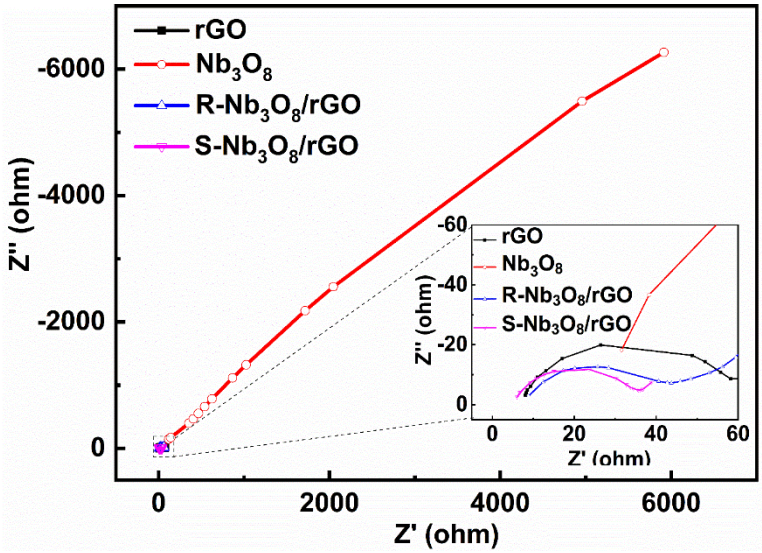

Figure S14. EIS of the rGO, Nb_3O_8 nanosheet, R-Nb_3O_8/rGO and S-Nb_3O_8/rGO electrodes after the potentiostatic process.

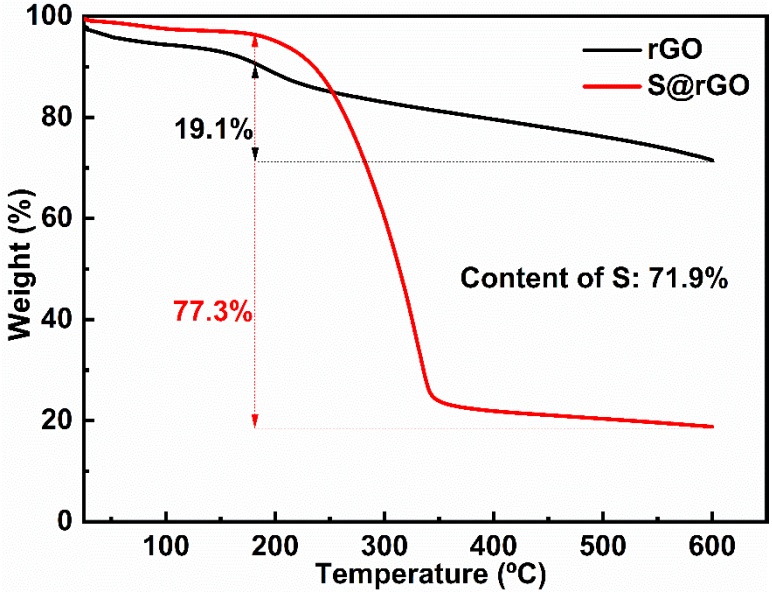

Figure S15. TG curves of rGO and S@rGO in a N_2 atmosphere.

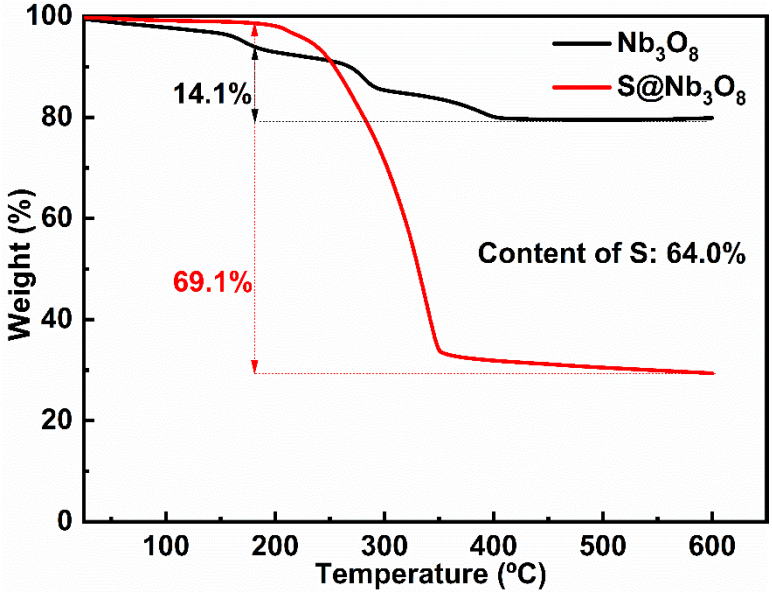

Figure S16. TG curves of Nb_3O_8 and S@Nb_3O_8 in a N_2 atmosphere.

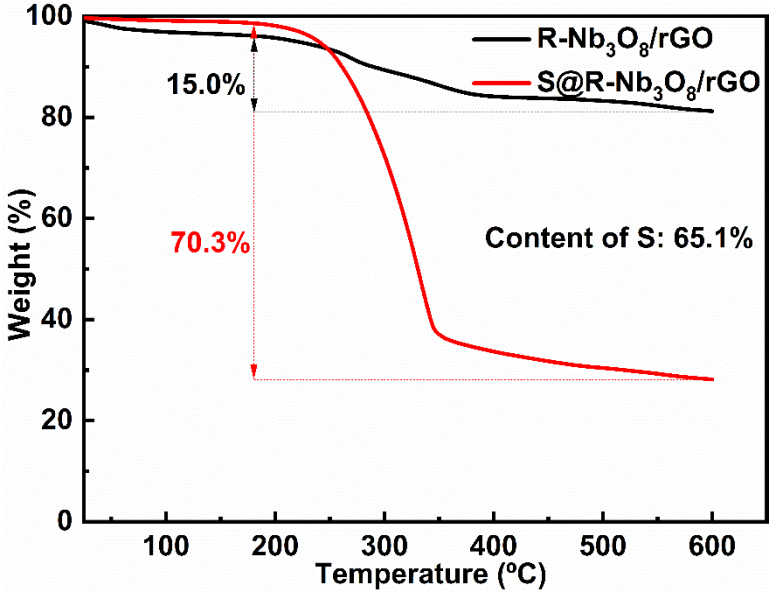

Figure S17. TG curves of R-Nb_3O_8/rGO and S@R-Nb_3O_8/rGO in a N_2 atmosphere.

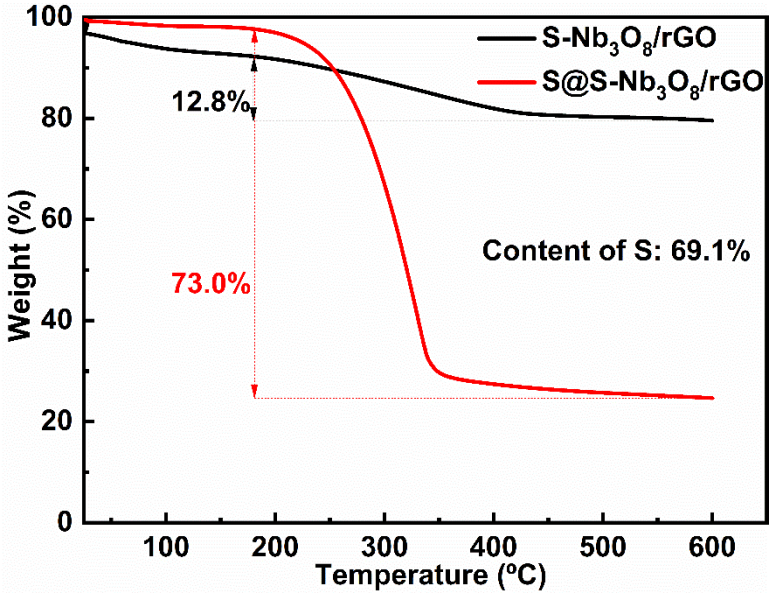

Figure S18. TG curves of S-Nb_3O_8/rGO and S@S-Nb_3O_8/rGO in a N_2 atmosphere.

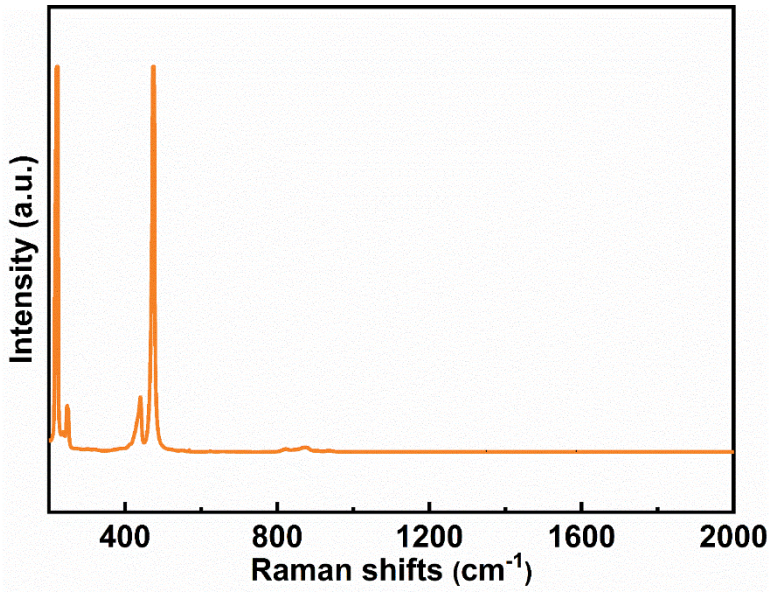

Figure S19. Raman spectrum of sulfur.

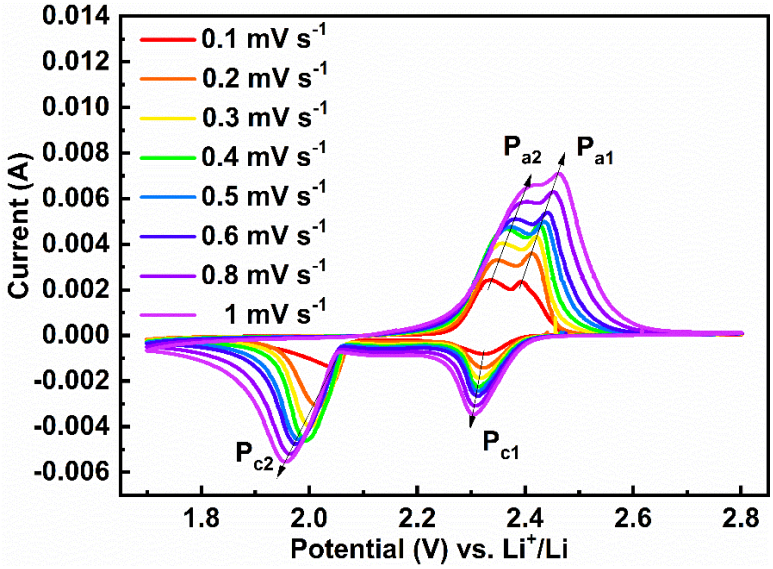

Figure S20. CV curves of the lithium sulfur battery assembled with the S@rGO sulfur cathode at different scan rates.

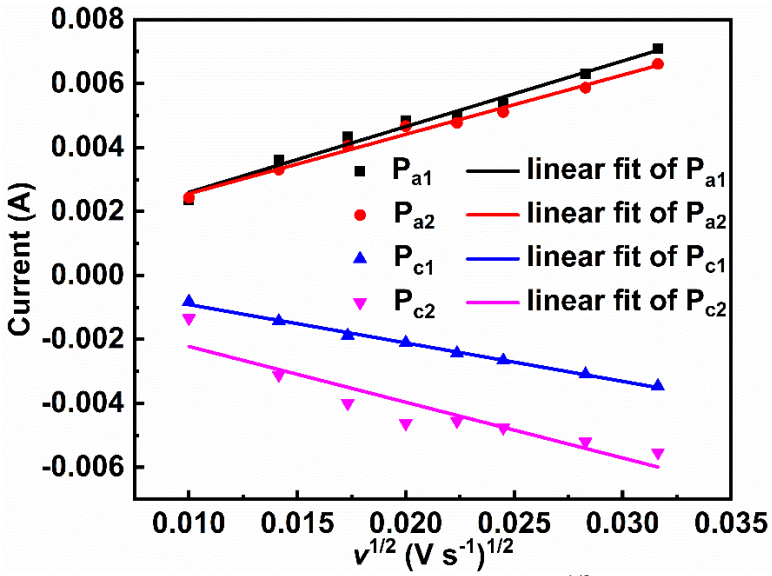

Figure S21. Linear fit curve of the peak current (I_P) against $v^{1/2}$ of S@rGO.

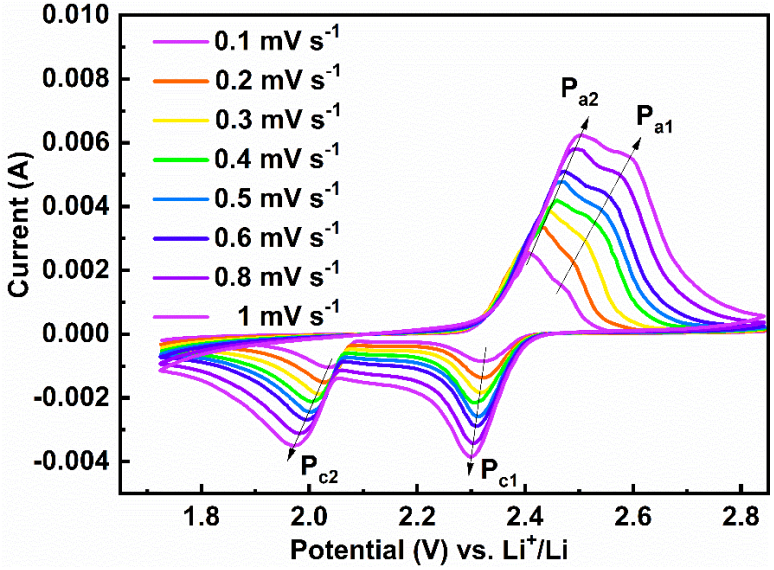

Figure S22. CV curves of the lithium sulfur battery assembled with the S@Nb_3O_8 sulfur cathode at different scan rates.

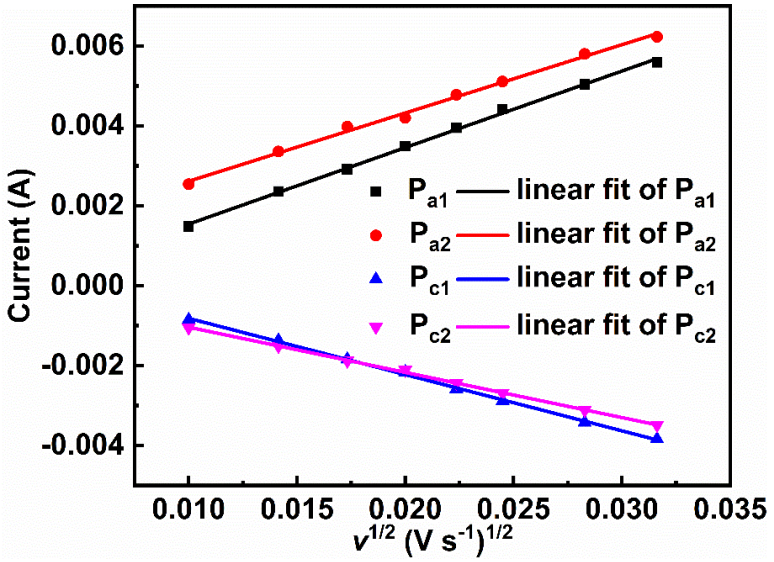

Figure S23. Linear fit curve of the peak current (I_P) against $v^{1/2}$ of S@Nb_3O_8.

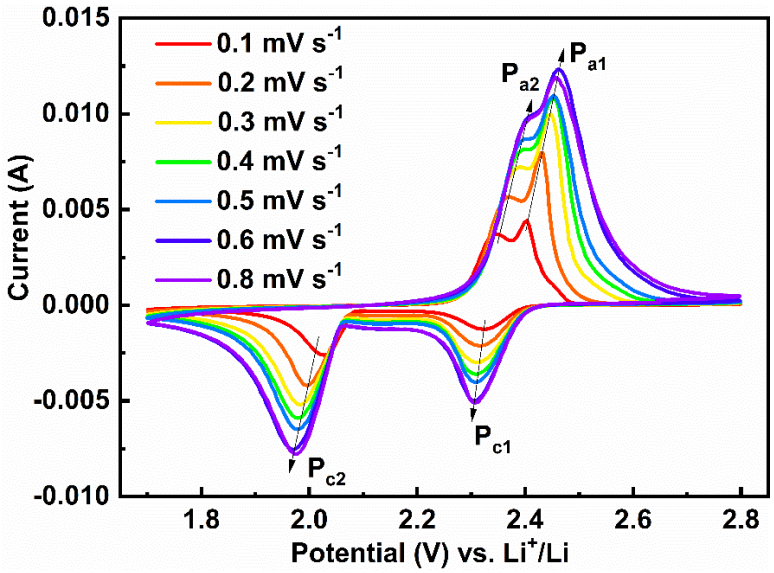

Figure S24. CV curves of the lithium sulfur battery assembled with the S@R-Nb_3O_8/rGO sulfur cathode at different scan rates.

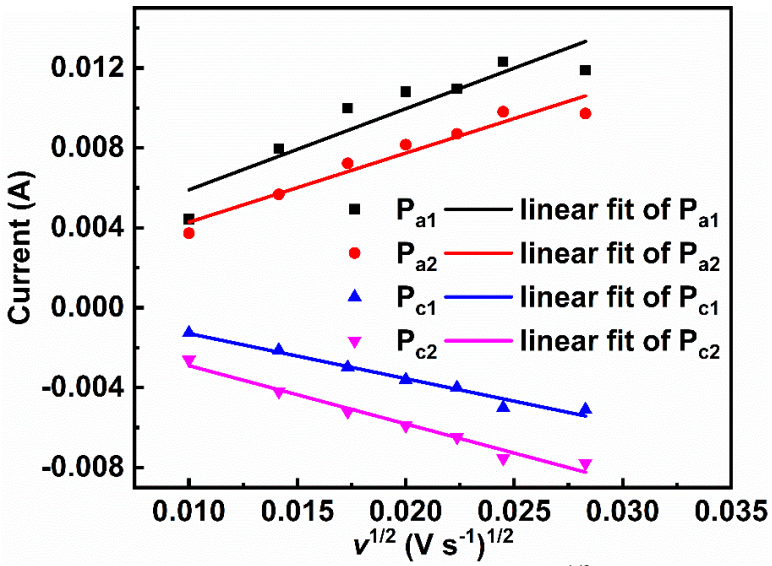

Figure S25. Linear fit curve of the peak current (I_P) against $v^{1/2}$ of S@R-Nb_3O_8/rGO.

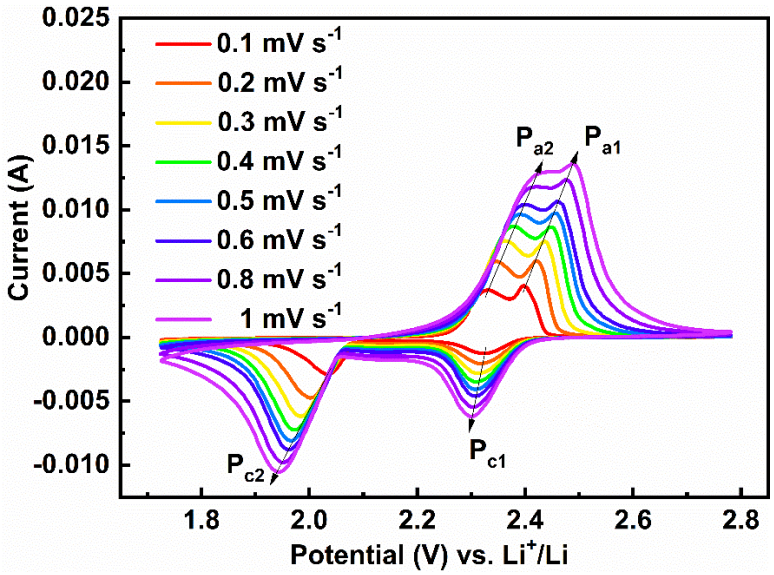

Figure S26. CV curves of the lithium sulfur battery assembled with the S@S-Nb_3O_8/rGO sulfur cathode at different scan rates.

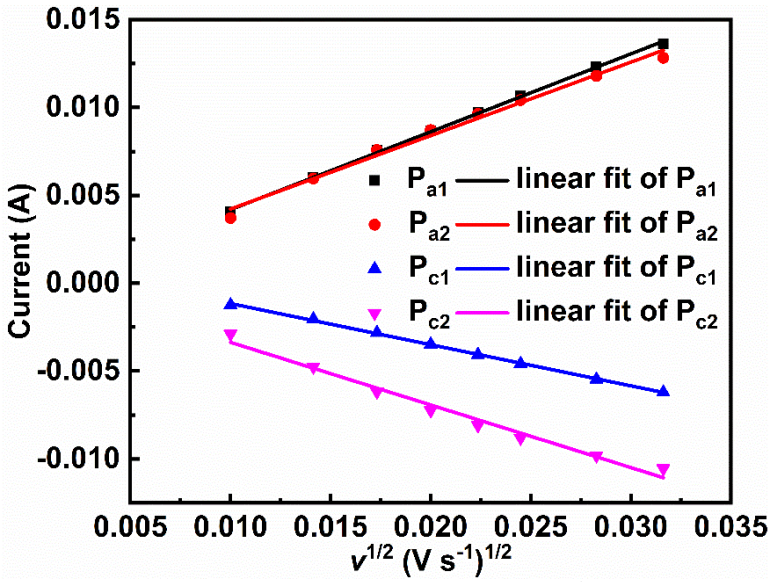

Figure S27. Linear fit curve of the peak current (I_P) against $v^{1/2}$ of S@-Nb_3O_8/rGO.

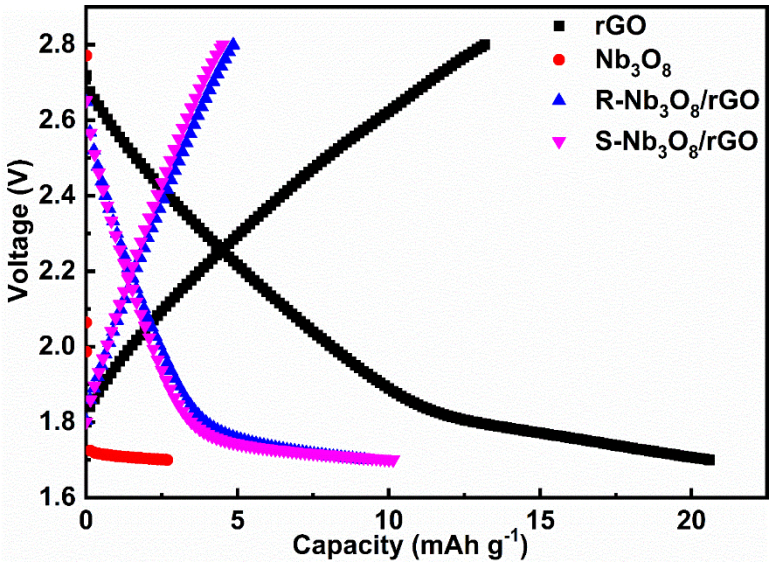

Figure S28. Galvanostatic charge/discharge curves of lithium batteries assembled with rGO, Nb_3O_8, R-Nb_3O_8/rGO and S-Nb_3O_8/rGO as cathode materials at 100 mA g^{-1}.

Table S1. Lithium sulfur battery performance of recently reported 2D host materials.

Electrode	0.1 C [mAh g^{-1}]	0.2 C [mAh g^{-1}]	0.5 C [mAh g^{-1}]	1 C [mAh g^{-1}]	2 C [mAh g^{-1}]	5 C [mAh g^{-1}]	10 C [mAh g^{-1}]	S Ratio [%]	Mass Loading [mg cm^{-2}]	Ref.
S@rGO	1000	625	500	450	410	115	/	50	1	This work
S@Nb_3O_8	500	375	250	200	170	62	/	50	1	This work
S@R-Nb_3O_8/rGO	1250	990	800	550	480	245	/	50	1	This work
S@S-Nb_3O_8/rGO	1529	975	867	793	726	647	528	50	1	This work
S@HNb_3O_8	NA	NA	NA	790	731	686	637	50	1.5	[7]
S@ Limonene	1160	1000	850	735	615	510	NA	37.5	1.8	[8]
S@Co/Carbon nanosheet	NA	1203	870	777	683	*594(3C) 549(4C)*	NA	56	1	[9]
S@Graphene	1265	1043	885	768	610	404	186	70	2	[10]
S@Graphene	1257	1050	900	760	680	609	450	63.2	2.4	[11]
S@MnO_2	1006.8	NA	662	569.8	496.9	NA	NA	65	0.65–1.06	[12]
S@Graphene/α-Fe_2O_3	NA	NA	NA	NA	NA	565	NA	NA	NA	[13]
S@MoS_{2-x}/RGO	NA	1310.5	1100	1050	950	900	*826.5(8C)*	75	1.5	[14]
S@MoS_2/RGO	NA	1243.2	940	900	830	600	*473.3(8C)*	75	1.5	[14]
S@MnO_2/HCF	*1160(0.05C)* 1090(0.1C)	1010	890	690	NA	NA	NA	71	3.5	[15]
S@NiO nanosheet	NA	1231	1050	890	801	696	NA	80	2.18	[16]
S@CH/LDH	900	800	650	500	NA	NA	NA	75	3	[17]
S@LDH	1375	1283	1139	1034	*783(3C)*	398	NA	55	4	[18]
S@LDH	*1192(0.05C)* 1080(0.1C)	980	860	790	709	NA	NA	70	1.2	[19]
S@LDH	1050	931	853	801	633	NA	NA	70	2-3	[20]
S@CNT/Ti_2C	NA	NA	1263	NA	NA	NA	NA	78/80	1-1.5	[21]

References

1 T. Nakato, N. Miyamoto and A. Harada, *Chem. Commun.*, 2004, DOI: 10.1039/b309628a, 78-79.

2 S. Park, J. An, R. D. Piner, I. Jung, D. Yang, A. Velamakanni, S. T. Nguyen and R. S. Ruoff, *Chem. Mater.*, 2008, **20**, 6592-6594.

3 P. Xiong, R. Ma, N. Sakai and T. Sasaki, *ACS Nano*, 2018, **12**, 1768-1777.

4 L. Li, R. Ma, Y. Ebina, K. Fukuda, K. Takada and T. Sasaki, *J. Am. Chem. Soc.*, 2007, **129**, 8000-8007.

5 K. Akatsuka, G. Takanashi, Y. Ebina, N. Sakai, M.-a. Haga and T. Sasaki, *J. Phys. Chem. Solids*, 2008, **69**, 1288-1291.

6 X. Cai, T. C. Ozawa, A. Funatsu, R. Ma, Y. Ebina and T. Sasaki, *J. Am. Chem. Soc.*, 2015, **137**, 2844-2847.

7 L. Xu, H. Zhao, M. Sun, B. Huang, J. Wang, J. Xia, N. Li, D. Yin, M. Luo, F. Luo, Y. Du,C. Yan, *Angew. Chem.-Int. Edit.*, 2019, **58**, 11491-11496.

8 F. Wu, S. Chen, V. Srot, Y. Huang, S. K. Sinha, P. A. van Aken, J. Maier and Y. Yu, *Adv. Mater.*, 2018, **30**, e1706643.
9 S. Liu, J. Li, X. Yan, Q. Su, Y. Lu, J. Qiu, Z. Wang, X. Lin, J. Huang, R. Liu, B. Zheng, L. Chen, R. Fu,D. Wu, *Adv. Mater.*, 2018, **30**, e1706895.
10 J. Xu, J. Shui, J. Wang, M. Wang, H.-K. Liu, S. X. Dou, I.-Y. Jeon, J.-M. Seo, J.-B. Baek and L. Dai, *ACS Nano*, 2014, **8**, 10920-10930.
11 J. L. Shi, C. Tang, H. J. Peng, L. Zhu, X. B. Cheng, J. Q. Huang, W. Zhu and Q. Zhang, *Small*, 2015, **11**, 5243-5252.
12 Q. Liu, J. Zhang, S. A. He, R. Zou, C. Xu, Z. Cui, X. Huang, G. Guan, W. Zhang, K. Xu and J. Hu, *Small*, 2018, **14**, e1703816.
13 C. Zheng, S. Niu, W. Lv, G. Zhou, J. Li, S. Fan, Y. Deng, Z. Pan, B. Li, F. Kang and Q.-H. Yang, *Nano Energy*, 2017, **33**, 306-312.
14 H. Lin, L. Yang, X. Jiang, G. Li, T. Zhang, Q. Yao, G. W. Zheng and J. Y. Lee, *Energy Environ. Sci.*, 2017, **10**, 1476-1486.
15 Z. Li, J. Zhang and X. W. Lou, *Angew Chem Int Ed Engl*, 2015, **54**, 12886-12890.
16 J. Wang, J. Liang, J. Wu, C. Xuan, Z. Wu, X. Guo, C. Lai, Y. Zhu and D. Wang, *J. Mater. Chem. A*, 2018, **6**, 6503-6509.
17 J. Zhang, H. Hu, Z. Li and X. W. Lou, *Angew. Chem.-Int. Edit.*, 2016, **55**, 3982-3986.
18 J.-Y. Hwang, H. M. Kim, S. Shin and Y.-K. Sun, *Adv. Func. Mater.*, 2018, **28**, 1704294.
19 H. J. Peng, Z. W. Zhang, J. Q. Huang, G. Zhang, J. Xie, W. T. Xu, J. L. Shi, X. Chen, X. B. Cheng and Q. Zhang, *Adv. Mater.*, 2016, **28**, 9551-9558.
20 J. Zhang, Z. Li, Y. Chen, S. Gao and X. W. D. Lou, *Angew. Chem.-Int. Edit.*, 2018, **57**, 10944-10948.
21X. Liang, Y. Rangom, C. Y. Kwok, Q. Pang and L. F. Nazar, *Adv. Mater.*, 2017, **29**, 1603040.